Exp.-Nr. A2-9/05
Eingang: 26.08.05
an PAC:

Mainz Microtron MAMI

Collaboration A2: "Real Photons"
Spokesperson: A. Thomas

Proposal for an Experiment

Helicity dependence of single and double pion photoproduction processes and the GDH integral on the neutron

Collaborators :

CrystalBall@MAMI collaboration

Spokespersons for the Experiment :

P. Pedroni, INFN-Sezione di Pavia

W. J. Briscoe, The George Washington University

A. Thomas, Institut für Kernphysik, Universität Mainz

Abstract of Physics :

We propose to measure the helicity dependence of the total inclusive photoabsorption process on the deuteron and the of quasi-free single and double pion photoproduction processes on the neutron at photon energies between 400 and 1400 MeV. The results of this experiment will greatly improve the experimental GDH integral value for the deuteron above 800 MeV and will provide important information on the resonance structure of the nucleon that can be directly compared to quark models in the framework of multipole analyses.

Abstract of Equipment :

We require a beam of tagged, circularly polarized photons incident on a longitudinally polarized deuteron. The 4π Crystal Ball photon spectrometer in combination with TAPS as a forward wall will be used. A threshold Cerenkov detector will be added for the on-line suppression of the background from electromagnetic events

MAMI–Specifications :

beam energy	855 and 1500 MeV
beam current	< 100nA
time structure	cw
polarization	circularly polarized photons

Experiment–Specifications :

experimental hall/beam	A2
detector	Crystal Ball, TAPS, MWPC, PID, Cerenkov
target material	polarized deuterated butanol

Beam Time Request :

set–up without beam	8 weeks
set–up/tests with beam	24 hours
data taking	350 hours at 855 MeV
data taking	450 hours at 1500 MeV
target repolarization	150 hours
data taking	200 hours at 1500 MeV with unpol. deuterium target (in conjunction with other experiments)

Helicity dependence of single and double photoproduction processes and the GDH integral on the neutron

Abstract

We propose to perform a precise measurement of the helicity dependence of the inclusive total absorption cross section on the deuteron and of the quasi free meson photoproduction with neutral final states using the Crystall Ball/TAPS set-up, complemented by the threshold Cerenkov counter, together wiht the Mainz new frozen-spin polarized target and the circularly polarizd MAMI-C photon beam. This measurement will give a much better insight into the GDH sum rule for the neutron and will allow an accurate investigation of the properties of the baryon resonances in the second and third region, and especially of the $D_{13}(1520)$, $D_{15}(1675)$ and $P_{33}(1600)$ states.

1 Introduction

The helicity dependent photoreaction data obtained for the first time at Mainz and Bonn by the GDH collaboration have greatly improved our knowledge of the γN interactions and of the nucleon properties.
The measurement of the total inclusive polarized cross section on the proton in the photon energy range 0.2-3 GeV [1, 2, 3] has provided the first experimental check of the Gerasimov-Drell-Hearn sum rule [4, 5], a well known fundamental theorem based on very general quantum mechanical principles. First data on the neutron have also been published [6, 7].
The double polarization data obtained at Mainz for the $\gamma p \to N\pi(\pi)$ channels [8, 9, 10, 11, 12, 13], have given a more accurate determination of some electromagnetic multipoles playing a relevant role in the first and second resonance region. In particular, the multipoles related to the excitation of the D_{13} resonance were determined with a greater accuracy than from all previous experiments. Additional results for partial reaction channels on the deuteron up to 800 MeV will also appear in future [14, 15, 16].
We propose to improve and extend the measurements performed on the deuterium, with a precise measurement of the helicity dependence of

- the total inclusive photoabsorption cross section on the deuteron in the photon energy range between 800 and 1400 MeV, where the statistical precision of the existing data is rather poor;
- the quasi-free $\gamma' n' \to n\pi^0(\pi^0)$ channels, between 400 and 1400 MeV, which could not be investigated by the previous measurements of the GDH collaboration.

2 Physical motivations

2.1 GDH sum rule on the neutron

The GDH sum rule deals with the absorption of circularly polarized photons by longitudinally polarized nucleons. The two relative spin configuration - parallel or antiparallel - determine the two absorption cross sections $\sigma_{3/2}$ (or σ_p) and $\sigma_{(1/2)}$ (or σ_a). They are connected to the nucleon anomalous magnetic moment κ in the following way:

$$I_{p,n}^{GDH} = \int_0^\infty \frac{d\nu}{\nu} (\sigma_p - \sigma_a) = \frac{2\pi^2 e^2}{m^2} \kappa_{p,n}^2 \tag{1}$$

where $\kappa_{p(n)}$ is the proton (neutron) anomalous magnetic moment, ν is the laboratory photon energy and m is the mass of the nucleon.
This sum rule, formulated in the 1960s, rests upon basic physics principles (Lorentz and gauge invariance, unitarity) and an unsubtracted dispersion relation applied to the forward Compton amplitude. Because of its fundamental character, it requires an experimental verification which has been awaiting technical developments that only recently have been achieved.
In Table 1 the measured value of the GDH integral for the proton are shown together with model predictions for the unmeasured energy ranges. The combination of the experimental result from MAMI and ELSA with the model predictions, yields to an estimate that is consistent with the GDH sum values within the experimental errors.

Table 1: Measured values of the GDH integral for the proton and model predictions for the unmeasured energy intervals

E_γ (GeV)		I_{GDH} (μb)
0.14-0.20	MAID03[17]	-29
	SAID[18]	-28
0.20-2.90	Measured[1, 2, 3] (Mainz+Bonn)	254±5±12
> 2.90	Simula et al.[19]	-13
	Bianchi-Thomas[20]	-14
TOTAL		$\simeq 215$
GDH sum rule		205

In the neutron case, the experimental situation is more complicated due to the lack of free neutron targets; deuteron or ^{3}He nuclei have to be used instead. Nuclear structure effects and final state interactions prevent the direct access to the free neutron cross sections and a theoretical support is needed for their evaluation.
The results obtained up to now at Mainz and Bonn for the helicity dependent total inclusive cross section on the deuteron are shown in fig. 1. The data from Mainz are still preliminary and evaluated using only a small fraction of the total available statistics. While more precise data are expected to come for $E_\gamma \leq 800$ MeV [21], the statistical precision of the final data obtained at higher energies is rather poor (see fig. 2) and need to be improved in order to make more stringent test of the different theoretical models.

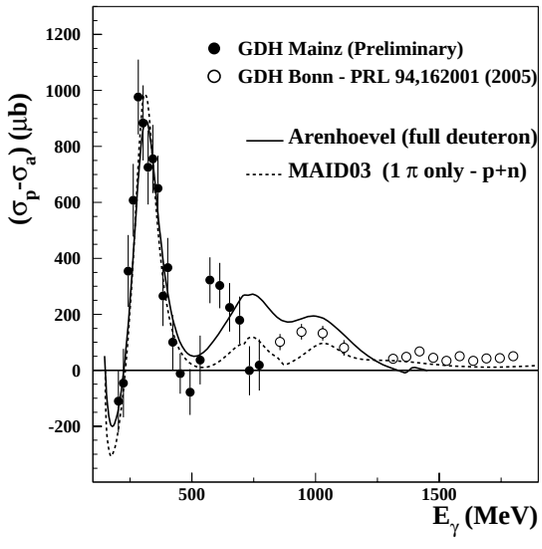

Figure 1: The helicity dependent inclusive total cross section on the deuteron obtained at Mainz and Bonn.

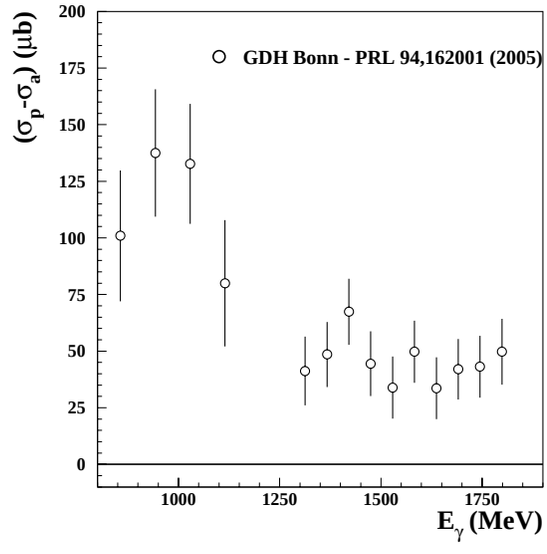

Figure 2: The helicity dependent inclusive total cross section on the deuteron obtained at Bonn.

In fig. 1, the experimental GDH deuteron results are also compared to the theoretical calculation of Arenhoevel, Fix and Schwamb [22], which represent the most comprehensive microscopic nuclear deuteron model available up to now. In this approach, the elementary $\gamma N \to N\pi(\pi)$ amplitudes on the free nucleons, are modified, within a coupled channel approach, to take into account both the nuclear effects due to the deuteron wave function and the final state interactions among the outgoing reaction particles. The amplitudes for the $\gamma N \to N\pi$ reactions are taken from the MAID multipole analysis [17] while for the $\gamma N \to N\pi\pi$ processes a phenomenological Lagrangian approach including resonance and Born contributions is used [23]. In the same figure, the MAID predictions for the free $N\pi$ processes are also shown for an estimation of the role played by nuclear effects in the Δ resonance region.

Discrepancies between the theoretical deuteron model and the experimental results can be clearly seen in the upper part of the measured energy region. Additional efforts are then needed to improve theoretical calculation in order to obtain a reliable derivation of the free-neutron helicity dependent cross section.
Above the Δ resonance region ($E_\gamma \gtrsim 500$ MeV) nuclear effects play a minor role, so that the difference between the deuteron and the proton, corrected by effects of the d-wave deuteron component, can be taken as a rough estimate for the spin asymmetry of the neutron. Preliminary analyses based on this idea show that the neutron behavior is similar to the proton one [7].
Also the status of the predictions for the helicity dependence of the free $\gamma N \to N\pi(\pi)$ reactions is far from being satisfactory as shown in table 2, where the last theoretical estimates of the GDH sum rule values for both proton and neutron are given. These estimates are derived from the SAID [18] multipole analysis of the available $N\pi$ data and from different estimates of the contribution given by the other relevant processes ($N\pi$, $N\eta$, $K\Lambda(\Sigma)$, $p\rho(\omega)$) up to $E_\gamma \simeq 2$ GeV. Above this photon energy interval, the contribution estimated from Regge-type approaches is also taken into account.

Table 2: Contributions of different partial reaction channels to the GDH sum rule. Predictions for $N\pi$ are from the [18] multipole analysis; estimates for $N\eta$ are from [17]; kaon channel contributions are from [24]; predictions for vector meson production are from [25]; Regge contributions are from [20].

Proton	I_{GDH} (μb)	Neutron	I_{GDH} (μb)
$\gamma p \to N\pi$	172	$\gamma n \to N\pi$	133
$\gamma p \to N\pi\pi$	94	$\gamma n \to N\pi\pi$	82
$\gamma p \to N\eta$	-8	$\gamma n \to N\eta$	-6
$\gamma p \to K\Lambda(\Sigma)$	4	$\gamma n \to K\Lambda(\Sigma)$	2
$\gamma p \to N\rho(\omega)$	0	$\gamma n \to N\rho(\omega)$	2
Regge contribution ($E_\gamma > 2$ GeV)	$\sim$ -15	Regge contribution ($E_\gamma > 2$ GeV)	$\sim$ 20
TOTAL	$\sim$ 240	TOTAL	$\sim$ 230
GDH sum rule	205	GDH sum rule	233

With respect to the previous estimates [1], this prediction still gives very different values from the "standard" GDH sum rule value for the proton but it is now reproducing the neutron GDH value. However, the (proton-neutron) difference has still a different sign with respect to the GDH prediction.
It is very instructive to perform the isospin decomposition of eq. 1 which results in:

$$I_{p,n}^{GDH} = \frac{2\pi^2 e^2}{m^2}(\kappa_s \pm \kappa_v)^2 = I_{vv} + I_{ss} \pm I_{vs} \qquad (2)$$

where the subscripts s, v denote the isovector and isoscalar parts of the anomalous magnetic moment, respectively. The dominance of the isovector component $\kappa_v = 1.85$ (in units of nuclear magnetons) over the isoscalar one $\kappa_s = -0.06$ is responsible of the extreme sensitivity of the isovector-isoscalar term I_{vs} in the GDH integral to the different models. This interference term is responsible for the $(p-n)$ difference of the sum rule.
Table 2 then points out the need of a precise test of the GDH sum rule both on the proton and on the neutron and of precise double polarization data for all $N\pi(\pi)$ channels, which give the dominant contribution to the GDH integral, in order to pin down the origin of the existing discrepancies.
For these reasons, we aim at

- a significant improvement of the statistical precision of the helicity dependent total inclusive photoabsorption data on the deuteron in the range 800-1400 MeV
- a precise measurement of the helicity dependent cross section of the quasi-free $\gamma n \to n\pi^0(\pi^0)$ channels

This program will be completed by the measurement of the helicity dependence for the $\gamma p \to N\pi(\pi)$ channels, which is presented in a parallel proposal [26].
In addition, measurements using a polarized ^{3}He gas target are also being planned. They will give further, important constraints to the nuclear models that are needed for evaluation of the free-neutron contribution. The feasibility studies of such a target are under way [27] and an additional proposal will be submitted in due time.

2.2 Single and double π^0 photoproduction on the neutron

Apart from the contribution to the GDH sum rule, the helicity dependence of the $N\pi^0$ channels provides an important testing ground for multipole models. Up to now estimates of the different multipole values are mostly based on unpolarized single pion photoproduction data, the great majority of which were taken on the proton. However, as clearly demonstrated by the results from the GDH collaboration [9], the polarization observables are a much better tool to disentangle the role of the different electromagnetic multipoles due to the change of sign of some contributions and to the presence of interference terms between different multipoles. For these reasons, the sensitivity to the smaller multipoles is greatly enhanced by the polarization observables and a precise determination of the photon coupling to the different nucleon resonances is then possible.
The planned measurement of the $n\pi^0$ channel (for which scarce data exist even in the unpolarized case) will in addition enable a complete characterization of the different isospin components of the multipole amplitudes and a better access to some resonant states as shown in figures 3 and 4. In these plots the MAID predictions of the helicity asymmetry E:

$$E = \frac{d\sigma_a - d\sigma_p}{d\sigma_a + d\sigma_p} = \frac{d\sigma_a - d\sigma_p}{(2 \cdot d\sigma_{unpolarized})} \tag{3}$$

for the $\vec{\gamma}\vec{p} \to p\pi^0$ and $\vec{\gamma}\vec{n} \to n\pi^0$ channels are displayed as a function of the photon energy at $\theta_{cm} = 90°$ and

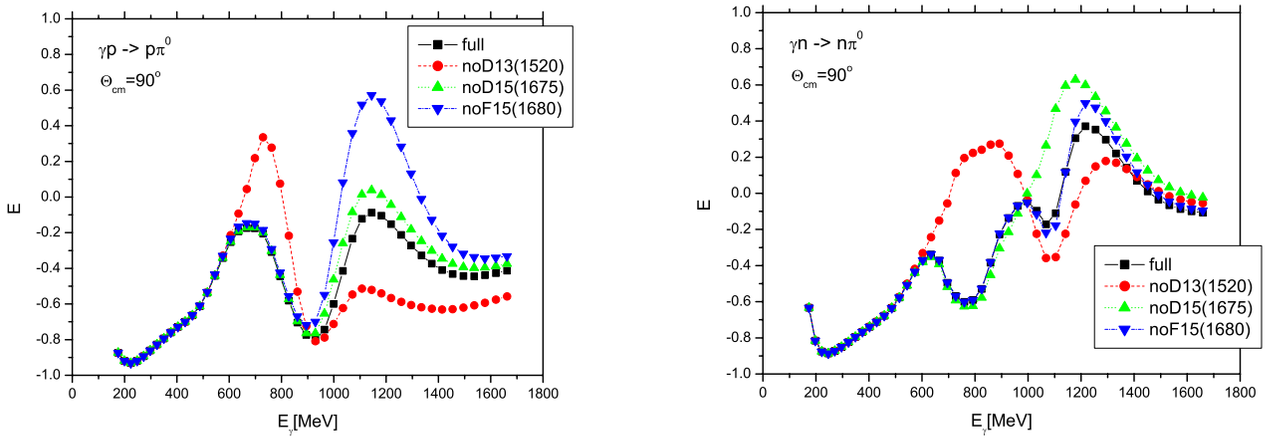

Figure 3: The sensitivity to the different resonances of the helicity asymmetry E for the $\vec{\gamma}\vec{p} \to p\pi^0$ (left) and $\vec{\gamma}\vec{n} \to n\pi^0$ (right) reactions at $\theta_{cm} = 90°$ as predicted by the MAID03 model.

$\theta_{cm} = 120°$ respectively, where θ_{cm} represents the pion angle in the center of mass system. The black (filled squares) curve represents the standard MAID03 solution while the other curves represent solutions in which the coupling constant of the denoted resonances were set to zero. The difference between the standard and modified solutions indicates the sensitivity of this observables to the different resonances.
While the sensitivity to the $D_{13}(1520)$ resonance is similar for both channels, the situation is completely different for the $D_{15}(1675)$ and $F_{15}(1680)$ resonances, for which the model predicts different helicity amplitudes between the two different nucleon states.
In table 3 the range of values for the helicity amplitudes $A_{1/2}$ and $A_{3/2}$ for these resonances is shown as predicted by the different $\gamma N \to N\pi$ partial wave analyses listed in the Review of Particle Physics [28]. The systematic differences between the analyses caused by using different parameterization schemes are indicative of the true uncertainties in the determination of these quantities: as it can be clearly seen from this table, our knowledge of the helicity amplitudes is still quite poor.
The combined measurements that are planned on different polarization observables both on the neutron and on the proton [26, 29, 30, 31] will then open a view on a completely new theoretical ground and unexpected characteristics of multipoles (or, in an equivalent way, of resonances) may very well appear. This has already been the case for the $\vec{\gamma}\vec{p} \to p\pi^0$ measurement performed by the GDH collaboration [9], which has given values of the helicity amplitudes for the D_{13} resonance in disagreement with all other $N\pi$ partial wave analyses.
The $n\pi^0\pi^0$ channels will provide additional and complementary information to the different baryon resonances [26]. Its sensitivity to the resonant states is enhanced with respect to the other $\gamma n \to N\pi\pi$ channels since

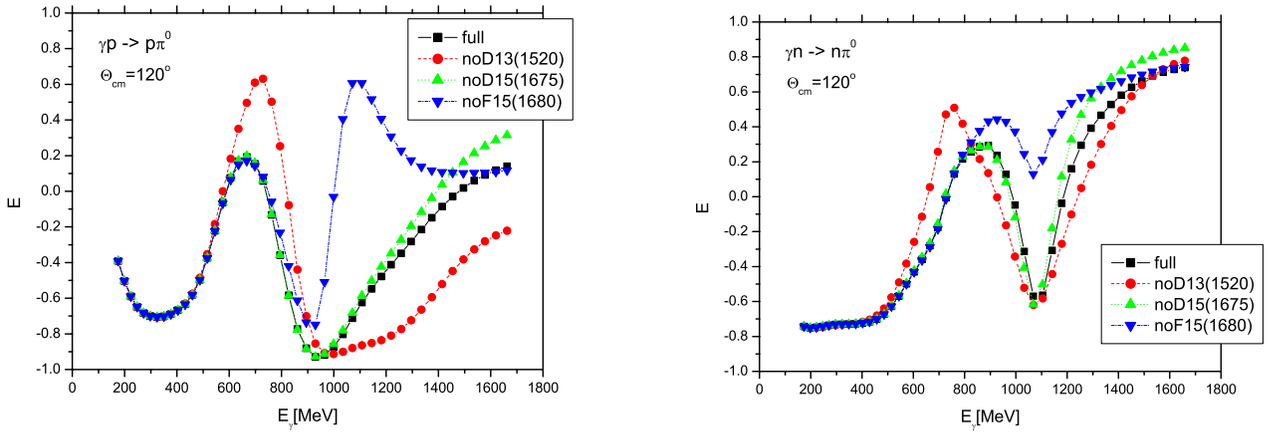

Figure 4: As in the previous figures but for at $\theta_{cm} = 120°$.

Table 3: Helicity amplitudes $A_{1/2}$ and $A_{3/2}$ for the $D_{13}(1520)$, $D_{15}(1675)$ and $F_{15}(1680)$ resonances.

	$D_{13}(1520)$		$D_{15}(1675)$		$F_{15}(1680)$	
	proton	neutron	proton	neutron	proton	neutron
$A_{1/2}$	[-38, -3]	[-84, -48]	[6, 34]	[-66, -21]	[-28, -5]	[17, 44]
$A_{3/2}$	[147, 178]	[-159, -118]	[3, 30]	[-30, -77]	[115, 154]	[-48, -23]

(units: $10^3 \cdot \mathrm{GeV}^{1/2}$)

the intermediate $\Delta\pi$ excitation term is strongly suppressed and, due to isospin conservation, no intermediate ρ contribution is also possible.
This reaction will be in particular very useful for those states having very large branching fractions to $N\pi\pi$ channels and small fractions to $N\pi$ channels. This is, for instance, the case of the $P_{33}(1600)$ resonance, that has an estimated $N\pi$ fraction of $10 - 25\%$ and an estimated $N\pi\pi$ fraction of $75 - 90\%$ [28].
The double polarization data obtained by th GDH colaboration for the $\gamma p \to N\pi\pi$ channels up to 800 MeV [10, 13, 32] could be described by the existing models only in a semi-quantitavive way due to the complicated nature of the underlying mechanisms. Also in this case, new data on both the proton and the neutron, will be essential to solve the existing discrepancies and to greatly improve our very poor knowledge of the $N\pi\pi$ reactions. A very useful tool for this kind of analyses will be given by the new partial wave formalism for these channel that has been recently developed by the Bonn group [33].

3 Experimental setup

3.1 The photon beam

The experiment will be carried out in the A2 hall using the tagged photon facility of the MAMI accelerator. Circularly polarized photons will be produced by bremsstrahlung of longitudinally polarized electrons [34]. The source of polarized electrons, based on the photoeffect on strained GaAs crystals, delivered routinely electrons with a degree of polarization of about 75%. Photons with a degree of polarization of more than 60% of the electron polarization are obtained in the upper half of the energy spectrum
The photon energies will be determined by the upgraded Glasgow tagging spectrometer, which will analyze the momenta of the electrons that have radiated bremsstrahlung photons. This detector system will able to tag photons in the range from 50 to 1400 MeV with a resolution of $\lesssim 4$ MeV.
As done before for the GDH experiment, the degree of polarization will be continuously measured during the whole experiment by Møller scattering on a magnetized iron foil. Both electrons were detected in coincidence inside the tagging system, which will then act in parallel as a Møeller spectrometer [35].

3.2 The target system

Longitudinally polarized deuterons will be provided by a frozen-spin deuterated butanol (C_4D_9OD) target that is presently under construction and that is expected to be operation in early 2007. This additional device will be very similar to the one that was successfully employed for the GDH experiment, both in Mainz and Bonn [36]. The system consists of a horizontal dilution refrigerator, presently under construction in DUBNA, and a superconducting polarization magnet, which will be used in the polarization phase together with a microwave system for dynamical nuclear polarization (DNP). During the measurement the polarization will be maintained in the "frozen spin" mode at temperatures of about 50 mK by an internal superconducting coil integrated into the dilution refrigerator. Thanks to a new doping material, during the last GDH measurement maximum polarization values higher than 70% were obtained for the deuterons at 2.5 T, with a relaxation time in the "frozen spin" mode higher than 100 hours (see figure 5) [15]. The holding field was homogeneous enough to allow for an accurate and continuous NMR monitoring of the the target polarization during the experiment.

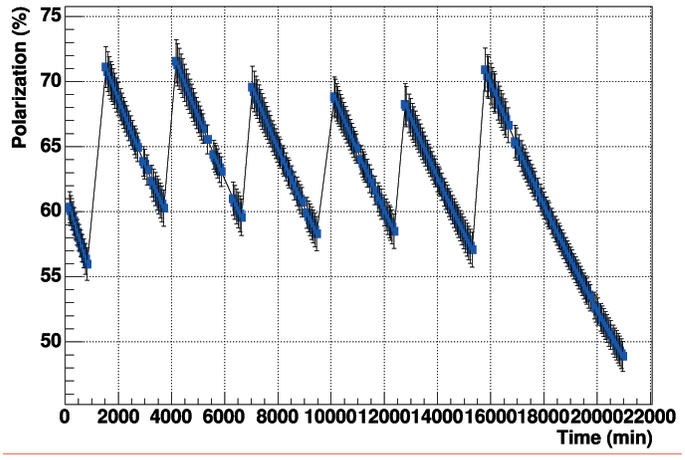

Figure 5: Time evolution of the polarization degree of deuterated butanol target during the 2003 GDH measurement in Mainz, as measured during a two weeks period.

3.3 The hadron detector

The previous GDH experiments at MAMI were carried out with a apparatus, based on the large acceptance detector DAPHNE, which was well suited for the detection of reactions having charged particles in the final state. The response for neutral particles was, however, limited. The energies and the emission angles of decay photons from π^0s and ηs could, for instance, not be measured.

The combination of the Crystal Ball (CB) and TAPS detectors (see figure 6) provides an almost 4π detector which is ideal to extend the previous measurement to multiphoton final states. This set-up has also a useful detection efficiency for neutrons, as shown in figures 7 and 8 were the measured neutron efficiency for CB and TAPS are respectively shown as a function of the neutron energy [37, 38].

The inclusion of a tracker detector composed by 2 cylindrical multiwire proportional chambers (MWPCs) and a thin cylindrical plastic scintillator barrel (PID) allows identification and energy measurement also for the charged particles, as shown by the two dimensional $dE/dX - E$ plot displayed in figure 9 [39]. The dE/dX information is given by the energy deposited in the PID detector corrected (using information from MWPC) for the path length, while the E information is given by the energy deposited in CB.

The separation between electron (dark region on the left corner) and pion (region enclosed inside the blue lines) zones can be clearly seen and, in addition, protons (region enclosed inside the red lines) can be still separated from charged pions up to kinetic energies of about 400 MeV.

The first production runs accomplished using the MAMI-B accelerators have confirmed the excellent properties of this set-up. As an example, In figures 10 and 11 the preliminary measured yields of the $\gamma p \to p\pi^0\pi^0$ and $\gamma p \to p\pi^+\pi^-$ are shown [42]. The shapes of both excitation functions are in very good agreement with the known cross section shapes for these reaction. This fact demonstrates that the detector response is well under control both for neutral and charged particles.

For the reasons that will be detailed later in sec. 4.1, for the measurement of the total inclusive cross section a threshold gas Cerenkov detector is needed to on-line suppress the events coming from electromagnetic (e.m.)

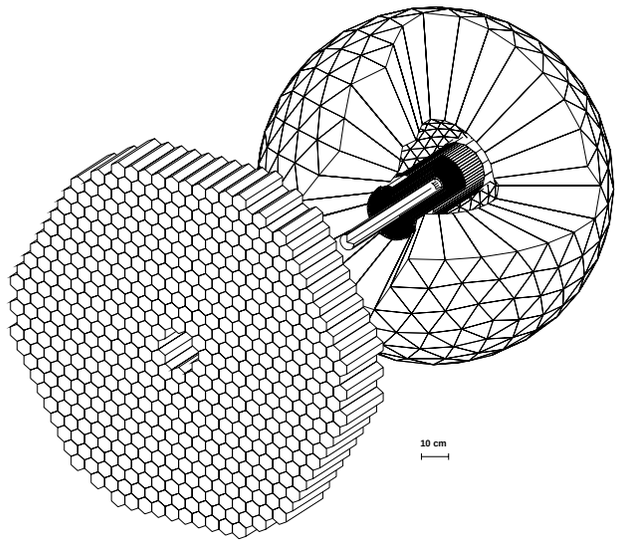

Figure 6: Schematic view of the CB-TAPS detector. Some of the CB crystals have been omitted to show the position of the PID-MWPC tracker detector and of the target.

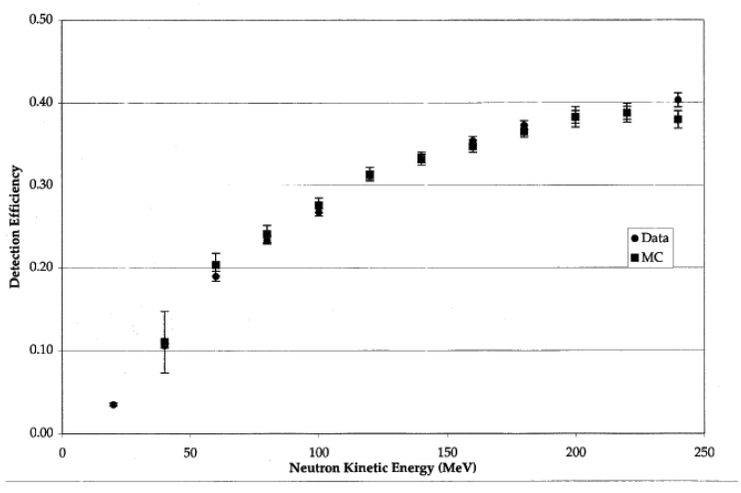

Figure 7: Neutron efficiency obtained with the CB detector using pion induced reactions [37].

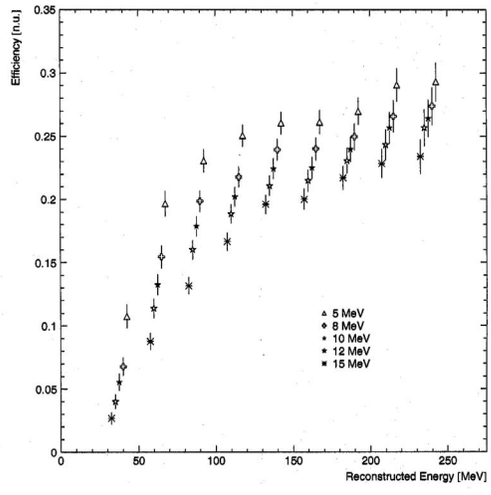

Figure 8: Neutron efficiency obtained with the TAPS detector as a function of the software energy threshold [38].

reactions inside the target. This detector will be installed between the CB frame and the TAPS detector to cover the angular polar region from 0° to 18°, where practically all e.m. events are emitted.
The aim of this apparatus is the detection of $e^{\pm}$ but not any hadronic reaction products. Since the lightest generated hadron is the pion ($m \simeq 140$ MeV) and the highest possible beam energy is about 1.5 GeV, it follows that the maximum possible kinetic energy for the pion will be close to about 1.4 GeV.
The Cerenkov light is emitted by particles having $\beta > 1/n$ (where n is the medium refractive index); it follows that a medium having $n < 1.004$ is needed in our case. A suitable gas is then C_4F_{10} ($n = 1.0014$), which has also a good transparency for the light in the UV range, where a large part of the Cerenkov radiation is emitted.
A schematic drawing of the complete detector geometry is shown in figure 12. This additional device will have a composite shape due to the need to use a part of the space inside the downstream part of the CB tunnel region, with a total volume of $\sim 1.3\text{m}^3$ and a light emission length along the z(beam)-axis (L_{rad}) of about 70 cm.
The gas volume will be enclosed in a light-tight aluminium casing where the entrance and exit windows consist of a thin foil. The Cerenkov light is focused via an ellipsoidal mirror onto a 5 inch photomultiplier tube (PMT). Both the mirror and the PMT will be the same as the ones used for the GDH experiment and the mechanical frame will be built in Gent be the same group that constructed the similar devices used by the GDH collaboration [41].

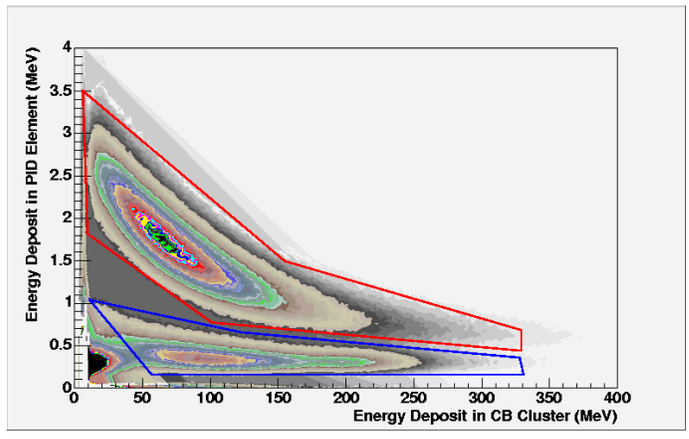

Figure 9: Experimental $dE/dX - E$ plot for charged particles photoproduced on ^{1}H.

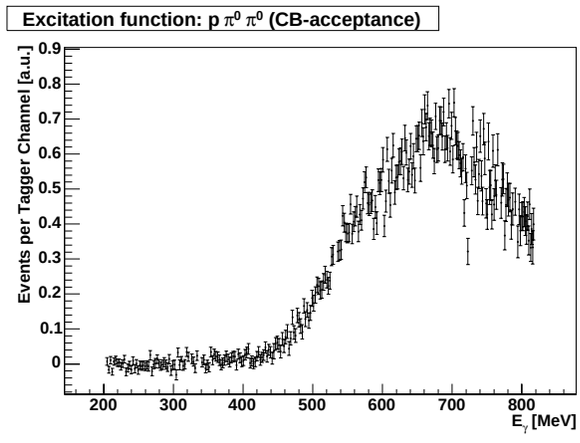

Figure 10: Preliminary easured yield of the $\gamma p \to p\pi^0\pi^0$ reaction.

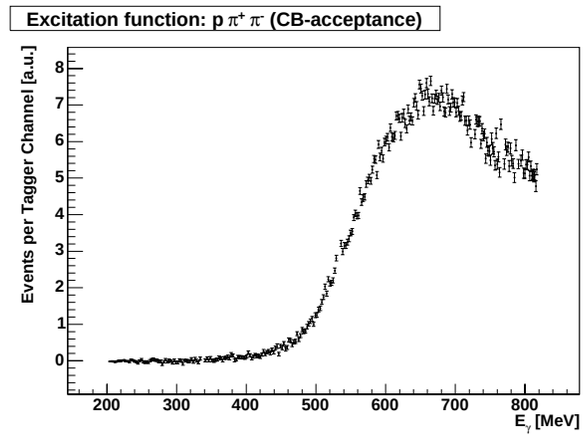

Figure 11: Preliminary measured yield of the $\gamma p \to p\pi^+\pi^-$ reaction.

The mirror, made out of perspex, has a central hole with a diameter of 5 cm for the passage of the photon beam. The hole is covered by a highly reflecting mylar foil in order to avoid losses of Cerenkov light. More technical details can be found in [40] A second, smaller planar mirror will be used to re-direct the light from the ellipsoidal mirror to the PMT entrance.
Results from a simulation, which takes into account the light propagation and reflection and the photocathode conversion probability are shown in figure 13. In the lower (upper) part of the figure the average number of photoelectrons $\langle N_{pe} \rangle$ created in the PMT (simulated $e^{\pm}$ detection efficiency) is shown as a function of the electron energy for different gas types (at 20° and 1 atm) and for $L_{rad} = 90\ cm$.
In order to reach efficiencies very close to 100%, a value $\langle N_{pe} \rangle \geq 12$ needs to be obtained. In the proposed configuration, $\langle N_{pe} \rangle \simeq 20$ is expected with a lower detection threshold for $e^{\pm}$ of about 10 MeV.
From test measurements made by the GDH collaboration in Mainz (medium: Aerogel+N_2) and Bonn (CO_2) efficiencies $\geq 99.99\%$ were found; similar values are also expected for this new device.

4 Experimental method

4.1 Total inclusive cross section measurement

For the considered photon energy range, photoabsorption processes lead to many different multiparticle final states which are very hard to detect individually with full acceptance and efficiency. To avoid large, systematic uncertainties arising from unobserved final states, the total photoabsorption cross section has to be measured inclusively, as done by the GDH collaboration both at Mainz and Bonn.
For this reason, it is necessary to observe at last one reaction product of all possible hadronic final states with almost complete acceptance as far as solid angle and efficiency are concerned. The corrections needed to evaluate

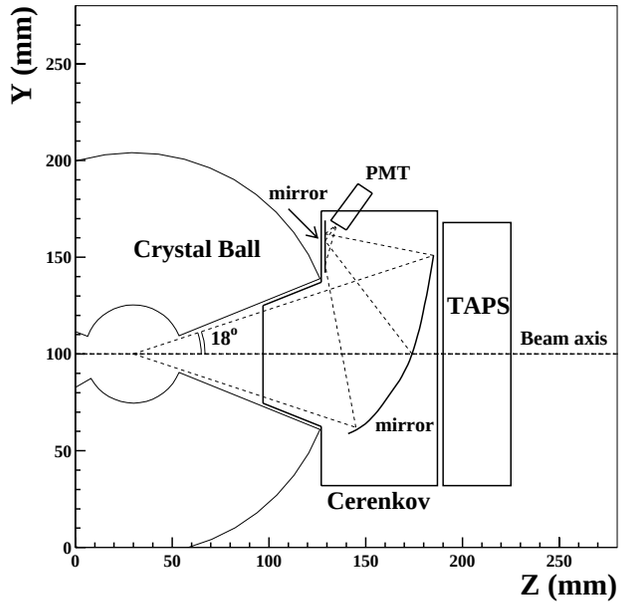

Figure 12: Schematic side view of the experimental setup including the Cerenkov detector.

the detector efficiencies and the loss of events emitted in the angular/momentum regions not covered by the detector have to be kept as low as possible to minimize model dependent contributions. The identification of individual processes is not necessary; what is needed is the reliable detection of charged particles and a high efficiency for the neutral decay modes of hadron. The CB-TAPS detector, with a covered solid angle of 97% of 4π and a detection efficiency $\gtrsim 99\%$ for both charged hadrons and γs coming from neutral meson decays, meets these requirements.

A very simple trigger condition, i.e. the presence of at least one (charged or neutral) particle inside CB or TAPS, needs then to be used for this measurement.

In figure 14 the simulated detector efficiency for all $N\pi$ channels is shown, under this condition, as a function of the pion angle in the center of mass system at $\mathrm{E}_\gamma = 1.0$ GeV. Neutron signals were not used for this evaluation; charged hadrons or photons with an energy release above a detection threshold of 40 MeV were taken into account.

These channels represents the worst case for the detector acceptance; when at least one additional pion is emitted in the final state, the efficiency is very close to 100% over the full angular range.

For the $n\pi^+$ channel, most unfavorable case, the unmeasured part of the cross section represents, in the unpolarized case, only $\simeq$2% of the total cross section for this channel and $\simeq$0.4% of the total inclusive cross section for the deuteron.

In order to minimize the errors associated to the extrapolation into the regions outside the detector acceptance the detector capabilities of isolating single reaction channels, both with neutral and charged particles in the final state, will be used both for the experimental evaluation of the main correction terms. and for a cross-check of the analysis procedure. The overall systematic error of the measurements can then be kept very low and will at least be of the same level as the ones of the GDH experiment ($\simeq$ a few % of σ_{tot}).

Due to the need of very loose trigger conditions, an essential part of the concept of the detector is the suppression of e.m. events, coming from pair production of electron and positron in the Coulomb field of the atomic nuclei and Compton scattering off orbital electron of the atoms, which represent the overwhelming part of the reaction products from the photon beam interactions with the target materials.

This background, which is by far more enhanced in forward direction than the hadronic events, has to be on-line suppressed by about 3 orders of magnitudes to gain access to the hadronic cross-section. This rejection will be performed with the aid of the Cerenkov counter located in the forward polar angular region that has been previously described in section 3.3.

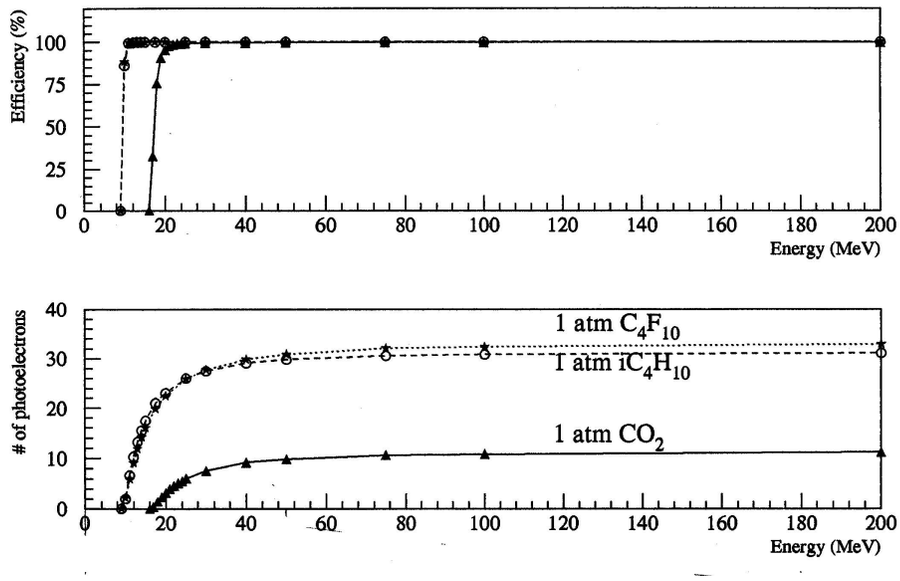

Figure 13: Simulated behavior of the Cerenkov detector (with $L_{rad} = 90$ cm) for different gas types at 20° and 1 atm. Lower plot: average number of photoelectrons created in the PMT; upper plot: $e^{\pm}$ detection efficiency.

4.2 Measurement of single and double photoproduction channels

The use of the Cerenkov detector will be very useful also for the partial channel measurements since it will allow to increase the accessible angular range into the forward polar region ($\theta < 20°$), where in general the strongest variations in cross sections and asymmetries can be found.
In this case the trigger conditions will be a combination of the standard cluster triggers requiring cluster multiplicities of 2 and and ≥ 3, since the channel identification requires the detection of all particles (neutron and γs from π^0 decay) in final state.
In figure 15, the θ_{cms} angular region available for the coincident detection of all final state particles is shown for the $n\pi^0$ reaction as a function of E_γ. Neutron detection was assumed to be effective for kinetic energies ≥ 50 MeV (see figures 7 and 8). Starting from $E_\gamma \simeq 350$ MeV, most of the angular region can be covered by the present apparatus.
As demonstrated by previous DAPHNE [43] and TAPS [44] data, final state interactions and nuclear effects do not play a relevant role for the quasi-free processes far from the π production threshold and the extraction of the free neutron information can be performed in a quite reliable way.
The situation for the $n\pi^0\pi^0$ is similar as before: simulations show that at $E_\gamma \simeq 600$ MeV almost 80% of the total phase space region can be accessed; this value rises to about 90% at $E_\gamma \simeq 1$ GeV to reach a maximum of about 95% at $E_\gamma \simeq 1.4$ GeV.
Due to the good capabilities for charged particle identification, the possibility of investigation of other quasi-free partial channels ($p\pi^-\pi^0$, $n\pi^+\pi^-$, ...) will be also explored.

5 Beam time estimate

The count rate estimate is based on the usual formula:

$$N_{tot} = (N_\gamma \cdot \Delta t) \cdot (f \cdot N_T) \cdot \epsilon_{det} \cdot \langle \sigma_{unpol} \rangle \tag{4}$$

where:

- N_{tot} is the total number of polarized events;
- N_γ is the photon flux for a given energy bin;
- Δt is the data taking (exposure) time;
- f is the target dilution factor;

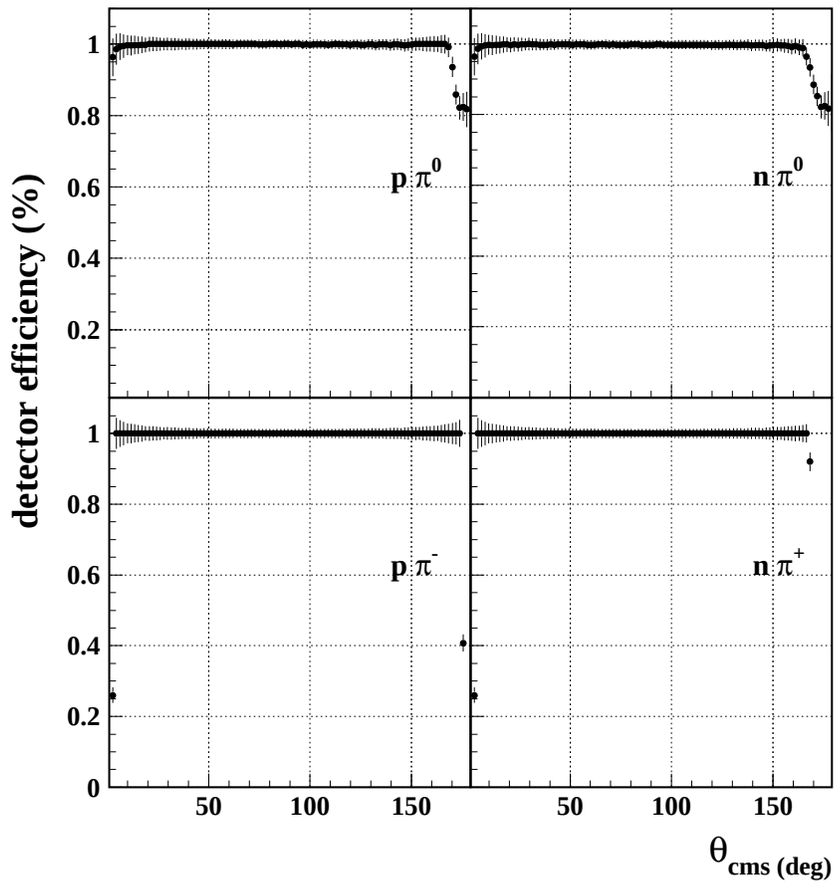

Figure 14: Simulated detection efficiency for all $N\pi$ channels at E_γ=1 GeV as a function of the π angle in the center-of-mass system.

- N_T is the number of target neutrons;
- ϵ_{det} is the detection and reconstruction efficiency;
- $\langle \sigma_{unpol} \rangle$ is the averaged cross section within the selected photon energy range.

The connection between the polarized cross difference $\Delta\sigma$ and the helicity asymmetry E is given as:

$$E = \frac{\sigma_p - \sigma_a}{\sigma_p + \sigma_a} \quad ; \quad \Delta\sigma = \sigma_p - \sigma_a = E * 2 * \sigma_{unpol} \tag{5}$$

which is used for the count rate estimate in each photon energy bin.
For each bin, the total number of measured events N_p and N_a for the two total helicity states is given by:

$$N_p = N_0(1 + PE + B + C) \tag{6}$$
$$N_a = N_0(1 - PE + B + C) \tag{7}$$

where

- N_0 is the number of unpolarized events
- $P = \langle P_\gamma \rangle \cdot \langle P_T \rangle$ is the product of the average values of beam and target polarization
- B is the background contribution due to unpolarized nucleons
- C is the background contribution due to the target cell

As described above, the average degree of polarization of the target is $\langle P_T \rangle = 0.6$ and that for photons $\langle P_\gamma \rangle = 0.6$, which yields $P = 0.36$. For a deuterated butanol target, $B = 3.2$ because of the dilution due to carbon and oxygen nuclei ($1/f = 1 + B$). The background due to the target cell amounts to C=4, as derived

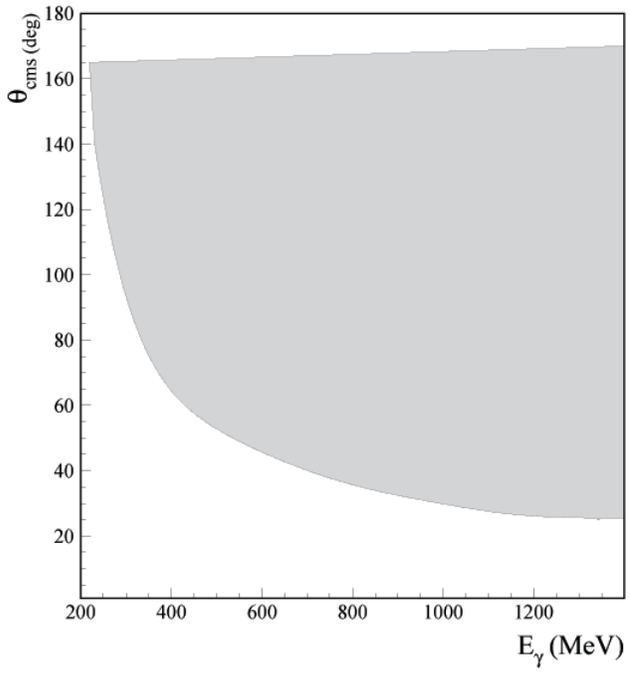

Figure 15: Covered kinematical region in (E_γ,θ_{cms}) for the $n\pi^0$ reaction.

from the previous DAPHNE runs. The combined effects of $P < 1$ and of the B and C background terms lead to a dilution of the measured asymmetry E_{meas}

$$E = \frac{\eta}{P} E_{meas} = \frac{\eta}{P} \cdot \frac{N_p - N_a}{N_p + N_a} \tag{8}$$

with $\eta = 1 + B + C$. The statistical uncertainty of E is then given by:

$$\delta E^2_{stat} = \frac{1}{P^2} \frac{\eta}{2N_0} \left[1 - \left(\frac{PE}{\eta} \right)^2 \right] \tag{9}$$

and (neglecting the small quadratic correction) the total number of events N_{tot} needed for both helicities state results:

$$N_{tot} = 2N_0 = \frac{\eta}{P^2} \cdot \frac{1}{\delta E^2_{stat}} \tag{10}$$

Combining eqs. 4 and 10, the estimated beam time is

$$\Delta t = \frac{\eta}{P^2} \frac{1}{\delta E^2_{stat}} [I_\gamma \cdot (f \cdot N_T) \cdot \epsilon_{det} \cdot \langle \sigma_{unpol} \rangle]^{-1} \tag{11}$$

The parameters entering the count rate estimate are:

- Incoming electron beam energy: $E_0 = 855$ and 1500 MeV;
- Tagged photon energy range: upper half of the photon energy range;
- A data acquisition capability of 1000 events/second is assumed, with an increase of a factor 2 compared to the existing readout due to a new S-link electronics. This gives an average tagged photon flux over the region of interest of $I_\gamma = 3.6 \cdot 10^5/(sec \cdot 20$ MeV)
- target nucleon density is $N_T \simeq 6 \cdot 10^{23}$ (cm^{-2}) for a 2 cm length;
- the target dilution factor amounts to $f = 20/84 = 0.24$ and $\eta = 8.2$;
- $P = \langle P_T \rangle \langle P_\gamma \rangle = 0.36$;
- $\epsilon_{app} \simeq 90$ is conservatively assumed for the total inclusive photoabsorption cross section;

- $\epsilon_{app} \simeq 20$ is assumed for the $n\pi^0$ case; this comes from the combination of the neutron efficiency (25%) and the π^0 reconstruction efficiency (80%).

For the total inclusive photoabsorption cross section we aim at a bin size of 20 MeV in photon energy and at a statistical precision of $\delta E_{stat} = 0.01$, which corresponds to an absolute uncertainty $\delta\Delta\sigma = \pm 5\mu$b for a cross section difference $\Delta\sigma = 50\mu$b. The required time to reach this goal in the energy range 800-1400 MeV ($\langle\sigma_{unpol}\rangle \simeq 150\mu$b) is 100 hours. This data taking will be performed in parallel with the partial channel measurement.
For the $n\pi^0$ process, we aim at a bin size of 20 MeV in photon energy and at 10 bins in the angular distribution with a statistical precision of $\delta E_{stat} = 0.05$, which corresponds to an absolute uncertainty $\delta\Delta\sigma = \pm 0.2\mu$b for a differential cross section difference $\Delta d\sigma/d\Omega = 1.5\mu/sr$. The required beam time to reach this goal in the in the energy range 800-1400 MeV ($\langle\sigma_{unpol}\rangle \simeq 1.5\mu$b$/sr$) is 450 hours. In the photon energy range 400-800 MeV ($\langle\sigma_{unpol}\rangle \simeq 2.5\mu$b$/sr$) 350 hours of beam time are also needed
The $n\pi^0\pi^0$ process is expected to have a smaller cross section, especially for photon energies below 1 GeV. In this case the energy bin size will be increased to $\Delta E_\gamma = \pm 20$ MeV, in order to reach similar values for δE_{stat} as before.
Based on the experience with the previous GDH experiment, additional 150 hours will be required for target polarization, photon flux and Møller measurements. Data with a liquid deuterium target will also be needed for unpolarized cross section data, but these can be measured in conjunction with other experiments.
To summarize, a total beam time of:

950 hours

is then requested for the asymmetry measurement of the total photoabsorption and the partial reaction channels on the polarized deuteron.

References

[1] J. Ahrens *et al.*, Phys. Rev. Lett. **87**, 022003 (2001).

[2] H. Dutz *et al.*, Phys. Rev. Lett. **91**, 192001 (2003).

[3] H. Dutz *et al.*, Phys. Rev. Lett. **93**, 032003 (2004).

[4] S.B. Gerasimov, Sov. J. Nucl. Phys. **2**, 430 (1966)

[5] S.D. Drell and A.C. Hearn, Phys. Rev. Lett. **16**, 430 (1966)

[6] A. Braghieri Nucl. Phys. **A 755**, 350c (2005)

[7] H. Dutz *et al.*, Phys. Rev. Lett. **93**, 162001 (2005).

[8] J. Ahrens *et al.*, Phys. Rev. Lett. **84**, 5950 (2000).

[9] J. Ahrens *et al.*, Phys. Rev. Lett. **88**, 232002 (2002).

[10] J. Ahrens *et al.*, Phys. Lett. **B 551**, 49 (2003).

[11] J. Ahrens *et al.*, Eur. Phys. J. A **A17**, 241 (2003)

[12] J. Ahrens *et al.*, Eur. Phys. J. A **21**, 323 (2004).

[13] J. Ahrens *et al.*, to be published in Phys.Lett.B.

[14] O. Jahn, PhD thesis, University of Mainz 2005.

[15] M. Martinez-Fabregate, PhD thesis, University of Mainz, in preparation;

[16] M. Blackston, PhD thesis, Duke University, NC (USA), in preparation.

[17] D.Drechsel, S.S. Kamalov, L. Tiator, Nucl. Phys. **A 645**, 145 (1999)

[18] R.A. Arndt *et al.*, Phys. Rev. C **66**, 055213 (2002).

[19] S. Simula *et al.*, Phys. Rev. D **66**, 034017 (2002).

[20] N. Bianchi and E. Thomas, Phys. Lett. **B 450**, 439 (1999).

[21] T. Rostomyan, PhD thesis, University of Gent, 2005.

[22] H.Arenhoevel, A. Fix and M. Schwamb, Phys. Rev. Lett. **93**, 202301 (2004).

[23] A. Fix and H.Arenhoevel, arXiv:nucl-th/0503042

[24] S. Sumowigado and T. Mart, Phys. Rev. C **60**, 028201 (1999)

[25] Q. Zhao, J.S. Al-Khalili and C. Bennhold, Phys. Rev. C **65**, 032201 (2002)

[26] J. Arends *et al.*, MAMI proposal, 2005

[27] P. Bartolome-Aguar, Diplomarbeit, University of Mainz, 2005 and Ph.D. thesis, University of Mainz, in preparation

[28] S. Eidelman *et al.*, Phys. Lett. **B 592**, 1 (2004),

[29] W.J. Briscoe *et al.*, MAMI proposal, 2005

[30] R. Beck *et al.*, MAMI proposal, 2005

[31] D. Watts *et al.*, MAMI proposal, 2005

[32] M. Lang, PhD thesis, University of Mainz, 2004.

[33] A.V. Anisovich *et al.*, Eur. Phys. J. A **24**, 111 (2005)

[34] K. Aulenbacher, Nucl. Instrum. Methods A **391**, 498 (1997).

[35] I. Preobajenski, Ph.D. thesis, University of Mainz, 2001.

[36] C. Bradtke *et al.*, Nucl. Instrum. Methods A **436**, 430 (1999).

[37] T.D. Stanislaus *et al.*, Nucl. Instrum. Methods A **462**, 463 (2001).

[38] M. Kotulla, Diplomarbeit, University of Giessen, 1997

[39] E. Downie, Ph.D. thesis, University of Glasgow, in preparation.

[40] B. Lannoy, Ph.D. thesis, University of Gent, 2000.

[41] , D. Ryckbosch, private communication.

[42] D. Krambrich, Ph.D. thesis, University of Mainz, in preparation.

[43] A. Zabrodin *et al.*, Phys. Rev. C **55**, R1617 (1997).

[44] J. Weiss *et al.*, Eur. Phys. J. A **16**, 275 (2003).